第 34 卷第 10 期 无 机 化 学 学 报 Vol.34 No.10
2018 年 10 月 CHINESE JOURNAL OF INORGANIC CHEMISTRY 1891-1898

席夫碱类三明治型铽/镝金属配合物的合成、表征及磁性

杨立国*,[1] 王 芳[1] 郁有祝[1] 王 鑫[1] 张永辉[1] 杨 华[2] 王大奇[2] 李大成[2]
([1]安阳工学院化学与环境工程学院,安阳 455000)
([2]聊城大学化学化工学院,聊城 252000)

摘要:以 *N*,*N*′-二(4-甲氧基水杨基)邻苯二胺(H_2L)为配体合成了 2 个新的稀土配合物[$M_2L_3(H_2O)$](M=Tb (**1**),Dy (**2**)),并对它们进行了红外分析、元素分析和单晶结构分析。单晶衍射结果表明,配合物 **1** 和 **2** 均为三明治型双核配合物。此外还研究了配合物 **1** 和 **2** 的磁学性质,结果表明配合物 **1** 和 **2** 都表现出反铁磁性作用和场诱导效应引起的慢弛豫行为。配合物 **2** 的有效能垒和弛豫时间分别为 35.45 cm^{-1} 和 2.7×10^{-10} s。

关键词:铽(Ⅲ)和镝(Ⅲ)配合物;席夫碱;晶体结构;磁学性质
中图分类号:O614.341;O614.342 **文献标识码**:A **文章编号**:1001-4861(2018)10-1891-08
DOI:10.11862/CJIC.2018.235

Sandwich-Type Tb and Dy Complexes with Schiff-Base Ligand: Syntheses, Crystal Structures and Magnetic Properties

YANG Li-Guo*,[1] WANG Fang[1] YU You-Zhu[1] WANG Xin[1]
ZHANG Yong-Hui[1] YANG Hua[2] WANG Da-Qi[2] LI Da-Cheng[2]
([1]*College of Chemistry and Environmental Engineering, Anyang Institute of Technology, Anyang, Henan* 455000, *China*)
([2]*School of Chemistry and Chemical Engineering, Liaocheng University, Liaocheng, Shandong* 252000, *China*)

Abstract: Two new sandwich-type di-lanthanide complexes [$M_2L_3(H_2O)$] (M=Tb (**1**), Dy (**2**), H_2L=*N*,*N*′-bis(4-methyloxysalicylidene)benzene-1,2-diamine) were synthesized by treating the Schiff-base ligand with $M(acac)_3\cdot6H_2O$ (M=Tb, Dy) and characterized by elemental analysis, IR spectra and X-ray single crystal diffraction. X-ray single crystal diffraction analysis reveals that **1** and **2** have a similar new triple-deck dinuclear sandwich structure. The magnetic measurements of complexes **1** and **2** indicated that **1** and **2** exhibit the antiferromagnetic interactions between lanthanide ions, and field-induced slow magnetic relaxation. The deduced effective energy barrier (U_{eff}) and relaxation time (τ_0) are 35.45 cm^{-1} and 2.7×10^{-10} s for **2**. CCDC: 1818315 **1**; 1818316, **2**.

Keywords: Tb(Ⅲ) and Dy(Ⅲ) complexes; Schiff base; crystal structures; magnetic properties

0 Introduction

Single Molecule Magnets (SMMs), first emerging in a dodecametallic manganese-acetate (Mn_{12}) with the slow relaxation of magnetization at low temperature[1-2], have attracted considerable attention due to the potential applications in high-density information storage[3], molecule-based spintronic devices[4], quantum computing devices[5] and refrigeration devices[6]. Two important factors for the design of SMMs involve the large spin ground state (*S*) and uniaxial (negative) magnetic anisotropy (*D*), leading to an anisotropy

收稿日期:2018-05-15。收修改稿日期:2018-07-14。
河南省科技攻关项目(No.182102210200)和安阳工学院校基金项目(No.YJJ2016014)资助。
*通信联系人。E-mail:lgyang@ayit.edu.cn,Tel:15670010482

energy barrier (U_{eff})[7]. With the large ground-state spin values, lots of polynunclear transition metal complexes have been synthesized as new SMMs to study the two ingredients (S and D)[8]. But in recent years, the lanthanide ions such as Dy(Ⅲ) and Tb(Ⅲ) are widely studied due to their large intrinsic magnetic anisotropy which increase the D values for the complexes resulting in higher energy barriers compared to SMMs with 3d metals[9]. So various lanthanide SMMs complexes have been synthesized, and one of the Dy SMMs has the largest effective energy barrier of 528 K in multinuclear SMMs[10]. In addition, the ligand field as well as the coordination geometry strongly influences the local anisotropy of the lanthanide ion. That is to say, the interplay between the ligand field effect, the geometry, and the strength of the magnetic interaction between the lanthanide sites will govern the SMM behavior[11]. Thus, it is necessary to study the magnetic interactions between the bridging ligand and the lanthanide ions.

Lots of organic ligands have been synthesized for discrete SMMs, for example, polyalcohols[10], carboxylic acid derivatives[12], oximate derivatives[13], and Schiff-base ligands[14]. These polydentate ligands can mediate the magnetic interactions between the metallic centers. Recently, several sandwich-type complexes with Schiff-base ligands have been reported[15], however, only one of them shows SMM behavior[16]. Furthermore, to the best of our knowledge, the sandwich-type complex with Schiff base ligand *N*,*N*′-bis(4-methyloxysalicylidene)benzene-1,2-diamine(H_2L) has not been reported.

In order to enlarge the structure database and further explore the magnetic interactions between the bridge group and lanthanide ions, two new triple-deckers sandwich complexes [$M_2L_3(H_2O)$] (M=Tb (**1**), Dy (**2**)) with Schiff base ligand have been synthesized and characterized by X-ray single crystal diffraction. Complexes **1** and **2** show the antiferromagnetic couple. The slow relaxation and strong quantum tunneling of magnetization exist for **1** and **2**. The deduced effective energy barrier(U_{eff}) and relaxation time (τ_0) of **2** are 35.45 cm^{-1} and 2.7×10^{-10} s.

1 Experimental

1.1 Chemicals and instruments

The ligand H_2L was prepared according to the published procedures[16]. All other reagents and solvents were used as received.

Elemental analyses were performed on an Elementar Vario MICRO CUBE elemental analyzer. Thermogravimetric analysis (TGA) experiments were carried out on a NETZSCH STA 449F3 thermal analyzer. IR spectrum was recorded as KBr discs on a Shimadzu IR-408 infrared spectrophotometer. Magnetic data was collected on magnetic measurement system MPMS-XL 7.

1.2 Synthesis of [$Tb_2L_3(H_2O)$] (1)

$Tb(OAc)_3\cdot6H_2O$ (199.2 mg, 0.2 mmol) and H_2L (112.9 mg, 0.3 mmol) were mixed in methanol (10 mL) in the presence of tetramethyl ammonium hydroxide. The solution was stirred for 5 h at room temperature and filtered. The filtrate was left undisturbed to allow slow evaporation of the solvent. Yellow single crystals suitable for X-ray diffraction were obtained after a week. Yield: 36 mg, 41.2% (based on Tb). IR (KBr cm^{-1}): 3 636 (br), 2 362 (s), 1 678 (s), 1 602 (m), 1 575 (s), 1 526 (s), 1 440 (vs), 1 381 (s), 1 357 (w), 1 310 (m), 1 234 (m), 1 201 (m), 1 116 (vw), 1 034 (vw), 971 (vw), 831 (w), 786 (vw), 735 (w), 650 (w), 612 (w). Anal. Calcd. for **1**·DMF ($C_{69}H_{63}Tb_2O_{14}N_7$, %): C, 54.08; H, 4.05; N, 6.40. Found(%): C, 54.11; H, 4.09; N, 6.35.

1.3 Synthesis of [$Dy_2L_3(H_2O)$] (2)

Complex **2** was obtained by following the procedure for **1** except that $Dy(OAc)_3\cdot6H_2O$ (199.9 mg, 0.2 mmol) was used instead of $Tb(OAc)_3\cdot6H_2O$. Yellow single crystals suitable for X-ray diffraction were obtained after a week. Yield: 30 mg, 40% (based on Dy). IR (KBr cm^{-1}): 3 652 (br), 2 989(s), 1 602(s), 1 578 (s), 1 524 (vs), 1 440 (s), 1 384(m), 1 312 (m), 1 299 (m), 1 183 (vw), 1 116 (vw), 1 029 (w), 978 (vw), 831 (w), 755 (w), 739 (w), 659 (w), 605 (w). Anal. Calcd. for $[Dy_2L_3(H_2O)]_4\cdot3DMF\cdot7H_2O$ ($C_{273}H_{259}Dy_8N_{27}O_{62}$, %): C, 52.75; H, 4.17; N, 6.09. Found (%): C, 52.67; H, 4.09; N, 6.11.

1.4 X-ray crystallography

The crystal data were collected on an Oxford Diffraction Gemini E system with a Cu $K\alpha$ sealed tube (λ=0.154 18 nm) at 296 K, using a ω scan mode with an increment of 0.3°. Preliminary unit cell parameters were obtained from 45 frames. Final unit cell parameters were derived by global refinements of reflections obtained from integration of all the frame data. The collected frames were integrated using the preliminary cell-orientation matrix. The SHELXL software was used for space group and structure determination, refinements, graphics, and structure reporting[17]. There are some large residual peak in complex **2**, and it is normal for the rare earth complexes. The crystallographic data and structural refinement parameters are provided in Table 1. Selected bond lengths and angles of complexes **1** and **2** are listed in Table 2.

CCDC: 1818315 **1**; 1818316, **2**.

Table 1　Crystallographic data for complexes 1 and 2

	1·DMF	$[Dy_2L_3(H_2O)]_4\cdot 3DMF\cdot 7H_2O$
Formula	$C_{69}H_{63}N_7O_{14}Tb_2$	$C_{273}H_{259}Dy_8N_{27}O_{62}$
Formula weight	1 532.09	6 210.06
Crystal system	Monoclinic	Monoclinic
Space group	$P2_1/c$	$P2_1/c$
a / nm	1.323 20(11)	2.580 4(3)
b / nm	2.766 1(2)	2.769 8(3)
c / nm	1.769 75(15)	1.943 7(2)
β / (°)	105.494 0(10)	91.146(2)
V / nm^3	6.242 2(9)	13.889(3)
Z	4	2
F(000)	2 904	5 816
D_c / (Mg·m^{-3})	1.550	1.399
μ / mm^{-1}	2.315	2.196
θ range / (°)	1.759~27.464	1.806~25.353
Reflection collected	66 827	126 678
Independent reflection	14 218 (R_{int}=0.041 2)	25 346 (R_{int}=0.059 6)
Parameter	791	1 595
R_1 [$I>2\sigma(I)$]	0.033 1	0.050 0
wR_2 [$I>2\sigma(I)$]	0.144 1	0.162 5
Goodness of fit	1.148	0.990

Table 2　Selected bond lengths (nm) and angles (°) for complexes 1 and 2

1					
Tb(1)-O(3)	0.223 2(3)	Tb(1)-N(3D)	0.256 1(4)	Tb(2)-O(8)	0.235 4(3)
Tb(1)-O(2)	0.232 4(3)	Tb(1)-N(5H)	0.258 2(4)	Tb(2)-N(7O)	0.246 6(4)
Tb(1)-O(8)	0.233 2(3)	Tb(1)-Tb(2)	0.385 47(4)	Tb(2)-N(2C)	0.249 4(4)
Tb(1)-O(6)	0.236 5(3)	Tb(2)-O(4)	0.222 1(3)	Tb(2)-O(7)	0.249 0(4)
Tb(1)-N(6L)	0.250 9(4)	Tb(2)-O(5)	0.222 4(3)		
Tb(1)-N(4F)	0.253 4(4)	Tb(2)-O(6)	0.233 1(3)		
O(3)-Tb(1)-O(2)	89.01(12)	O(2)-Tb(1)-N(6L)	72.97(13)	N(6L)-Tb(1)-N(4F)	63.06(13)
O(3)-Tb(1)-O(8)	83.07(11)	O(8)-Tb(1)-N(6L)	151.72(12)	O(3)-Tb(1)-N(3D)	79.13(13)
O(2)-Tb(1)-O(8)	86.57(11)	O(6)-Tb(1)-N(6L)	86.22(11)	O(2)-Tb(1)-N(3D)	155.27(13)
O(3)-Tb(1)-O(6)	148.27(12)	O(3)-Tb(1)-N(4F)	72.49(13)	O(8)-Tb(1)-N(3D)	70.62(13)

Continued Table 1

O(2)-Tb(1)-O(6)	74.50(11)	O(2)-Tb(1)-N(4F)	116.63(12)	O(6)-Tb(1)-N(3D)	104.80(12)
O(8)-Tb(1)-O(6)	69.29(11)	O(8)-Tb(1)-N(4F)	145.21(12)		
O(3)-Tb(1)-N(6L)	115.09(12)	O(6)-Tb(1)-N(4F)	139.14(12)		
		2			
Dy(1)-O(18)	0.220 7(5)	Dy(1)-Dy(2)	0.384 37(6)	Dy(2)-O(16)	0.235 2(4)
Dy(1)-O(19)	0.219 1(5)	N(1)-Dy(4)	0.252 7(6)	Dy(2)-N(7)	0.248 5(6)
Dy(1)-O(16)	0.233 8(4)	O(1)-Dy(4)	0.234 2(5)	Dy(2)-N(9)	0.252 4(5)
Dy(1)-O(15)	0.236 6(4)	O(1)-Dy(3)	0.237 5(4)	Dy(2)-N(8)	0.252 4(6)
Dy(1)-O(25)	0.239 8(5)	Dy(2)-O(14)	0.222 1(4)	Dy(2)-N(10)	0.254 4(5)
Dy(1)-N(11)	0.245 4(6)	Dy(2)-O(13)	0.229 5(5)		
Dy(1)-N(12)	0.247 5(5)	Dy(2)-O(15)	0.232 6(4)		
O(18)-Dy(1)-O(19)	92.2(2)	O(18)-Dy(1)-O(25)	89.99(19)	O(16)-Dy(1)-N(11)	103.18(19)
O(18)-Dy(1)-O(16)	160.15(17)	O(19)-Dy(1)-O(25)	80.87(18)	O(15)-Dy(1)-N(11)	81.05(18)
O(19)-Dy(1)-O(16)	105.15(19)	O(16)-Dy(1)-O(25)	83.42(17)	O(25)-Dy(1)-N(11)	151.19(19)
O(18)-Dy(1)-O(15)	90.64(17)	O(15)-Dy(1)-O(25)	75.03(17)	O(18)-Dy(1)-N(12)	117.28(19)
O(19)-Dy(1)-O(15)	155.73(18)	O(18)-Dy(1)-N(11)	74.3(2)		
O(16)-Dy(1)-O(15)	69.59(15)	O(19)-Dy(1)-N(11)	122.9(2)		

2 Results and discussion

2.1 Structure description

Complexes **1** and **2** crystallize in the monoclinic system with the similar structure. Herein, the molecular structure of complex **2** is described in detail as a representative example. As shown in Fig.1b, complex **2** is a triple-decker sandwich structure containing three Schiff base ligands, two Dy(Ⅲ) ions and one water molecule. One Dy(Ⅲ) ion is eight-coordinated and bridges two neighboring Schiff base ligands by four O atoms and four N atoms, while the other one is seven-coordinated by N_2O_2 cavity of one outer Schiff base ligand, two oxygen atoms of the inner common Schiff base ligand, and one oxygen atom of additional water molecule. The average bond distances of Dy1-O and Dy1-N are 0.229 8 and 0.251 2 nm, respectively, which are similar to the corresponding distances of the reference reported[16]. The average distances between Dy and the N_2O_2 planes are 0.133 nm, which is almost consist with the reference[16]. The separation between the two intramolecular Dy(Ⅲ) ions amounts to 0.385 5 nm for **2**, while the separation is 0.383 9 nm for **1**, indicating the presence of intramolecular interionic magnetic interaction in terms of the metal-metal separation, which is almost consist with the similar complex reported[16].

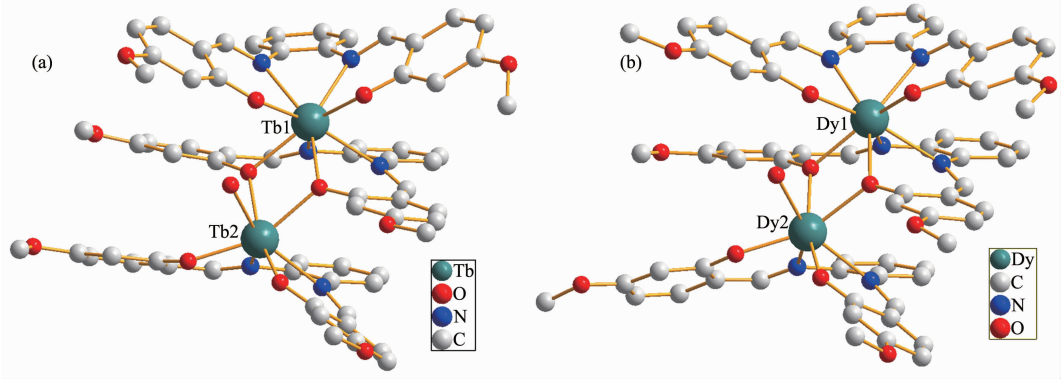

Fig.1 Molecular structures of **1** (a) and **2** (b)

2.3 Thermal stability

Thermal stability is an important aspect for the application of coordination complex. Thermogravimetric analysis (TGA) experiments were carried out to determine the thermal stabilities of **1** and **2** (Fig.2). For complex **1**, there are solvent molecules including DMF molecules and water molecules coordinated in the structure, and TG curve showing the first consecutive step of weight loss was observed in the range of 40~200 ℃, corresponding to the release of solvent molecules. Then, the continuously weight loss corresponds to the release of ligands (in the range of 180~800 ℃). For **2**, TG curve showing the first consecutive step of weight loss was observed in the range of 40~200 ℃, corresponding to the release of solvent molecules. Then, the continuously weight loss corresponds to the release of ligands in the range of 300~600 ℃.

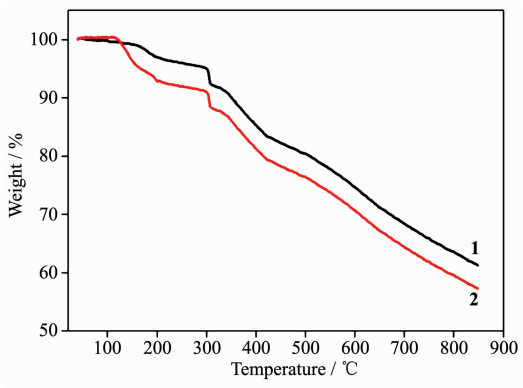

Fig.2　TG curves of complexes **1** and **2**

2.4 Magnetic studies

The variable-temperature dc magnetic susceptibility measurement for complexes **1** and **2** were performed in the temperature range of 2~300 K under an applied magnetic field of 1 000 Oe. The collected data are plotted as $\chi_M T$ vs T in Fig.3. The $\chi_M T$ values of **1** and **2** are 24.15 and 28.06 $cm^3 \cdot K \cdot mol^{-1}$ at 300 K, respectively, which are consistent with the expected values of 23.64 $cm^3 \cdot K \cdot mol^{-1}$ for two Tb(Ⅲ) ions ($^7F_6$, S=3, L=3, g=4/3)[18] and 28.34 $cm^3 \cdot K \cdot mol^{-1}$ for two Dy(Ⅲ) ions ($^6H_{15/2}$, S=5/2, L=5, g=4/3)[19]. With the temperature decreasing, the $\chi_M T$ value of **1** almost keeps a constant until 50 K, and then drops rapidly to 8.62 $cm^3 \cdot K \cdot mol^{-1}$ at 2 K, and the $\chi_M T$ value of **2** decreases rapidly to 14.36 $cm^3 \cdot K \cdot mol^{-1}$ from 10 to 2 K, which is mostly due to the thermal depopulation of the Stark sublevels and/or significant magnetic anisotropy in Tb^{3+}/Dy^{3+} ion systems. Compared to the complexes with similar structure without the radical contribution [20-21], it indicates the presence of antiferromagnetic coupling between the two Tb/Dy ions for **1** and **2**, respectively.

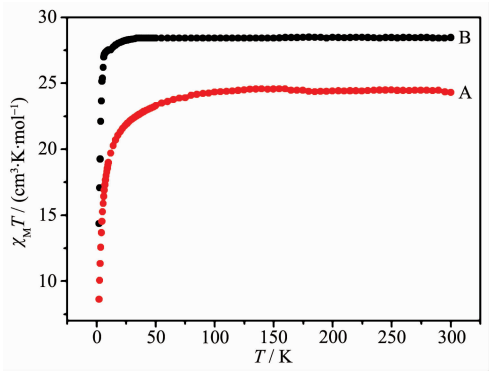

Fig.3　Temperature (T) dependence of $\chi_M T$ for **1** (A) and **2** (B) at 1 000 Oe

In addition, the magnetic-field-dependent magnetic properties of **1** and **2** have been studied. As shown in Fig.4, three observed non-superposition curves for **1** and **2** display a rapid increase at low field and eventually achieve the maximum value of 11.02μ_B~11.17μ_B for **1** and 13.90μ_B~13.91μ_B for **2** at 4 T, without reaching the theoretical magnetization saturation(18μ_B for two Tb(Ⅲ) ($^7F_6$, S=3, L=3, g=3/2) ions and 20μ_B for two Dy(Ⅲ) ($^6H_{15/2}$, S=5/2, L=5, g=4/3) ions, respectively), revealing the crystal-field effect on the Dy(Ⅲ) and Tb(Ⅲ) ions in the two triple-decker complexes.

To explore the dynamic magnetic property of the complexes, the temperature dependence of the alternating-current (ac) magnetic susceptibility of **1** and **2** under a zero direct-current (dc) magnetic field oscillating at 10~997 Hz is recorded in Fig.5~6. As can be seen, **1** and **2** exhibit the frequency-dependent character in the out-of -phase (χ'') signals, indicating the slow relaxation of magnetization, which is generally attributed to the SMM nature of the two complexes. However, the frequency-dependent behavior was not observed in the in-phase (χ') signals for **1** and **2**.

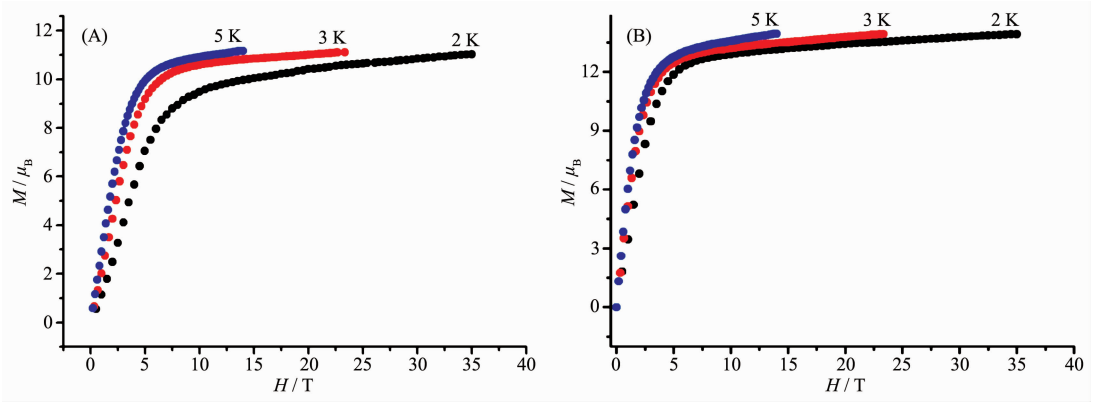

Fig.4 Plots of M vs H/T for **1** (A) and **2** (B) at different temperatures

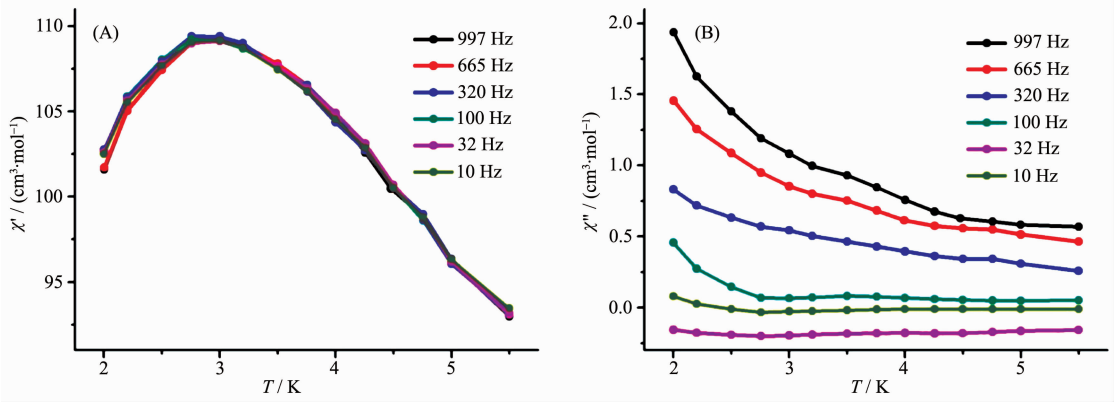

Fig.5 Plots for temperature dependence of the in-phase (χ') (A) and out-of-phase (χ'') (B) ac susceptibility of **1** under zero applied dc magnetic field

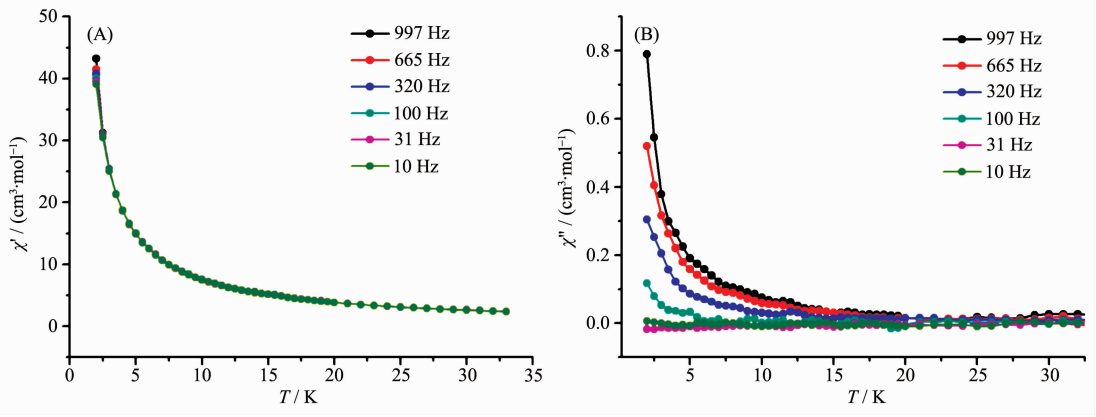

Fig.6 Plots for temperature dependence of the in-phase (χ') (A) and out-of-phase (χ'') (B) ac susceptibility of **2** under zero applied dc magnetic field

Furthermore, the peak was not observed in out-of-phase (χ'') signals for **1** and **2**, which suggests the strong effect of quantum tunneling of magnetization (QTM).

To reduce the effect of QTM, an optimal direct-current field of 2 000 Oe was applied to the dynamic measurement over **1** and **2**. As expected, the frequency-dependent character is still exist in both of the in-phase (χ') and out-of-phase (χ'') signals for **1** and **2**, further confirming the SMM nature of the two complexes, as shown in Fig.7. In addition, the peak of the out-of-phase signal (χ'') for **2** could be observed until a frequency as low as 10 Hz, indicating the effective suppression of quantum tunneling of

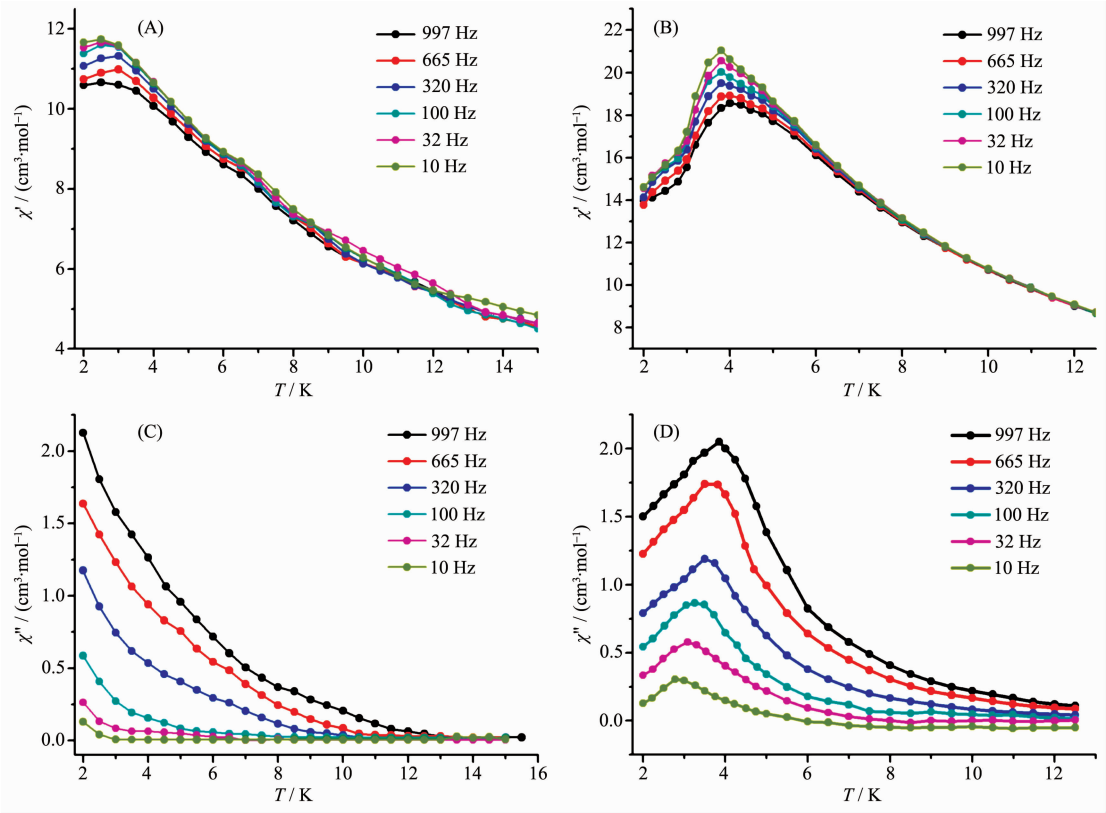

Fig.7　Plots for temperature dependence of the in-phase (χ') and out-of-phase (χ'') ac susceptibility of **1** (A, B) and **2** (C, D) under 2 000 Oe applied dc magnetic field

magnetization (QTM) under an applied 2 000 Oe magnetic field. On the basis of a thermally activated mechanism, $\tau=\tau_0\exp[U_{eff}/(kT)]$ and $\tau=1/(2\pi\nu)$, the Arrhenius law fitting for the data under a 2 000 Oe magnetic field was carried out. As shown in Fig.8, a linear relationship exists between $\ln\tau$ and $1/T$ in the temperature range of 2.7~3.8 K for **2**, which in turn result in a barrier U_{eff}=35.5 cm^{-1} (51.0 K) and $\tau_0=2.7\times10^{-10}$ s with R=0.98. However, the relaxation time and energy barrier of slow magnetic relaxation cannot be deduced for **1**, most probably because of the stronger tunneling effect of complex **1** in comparison with **2**.

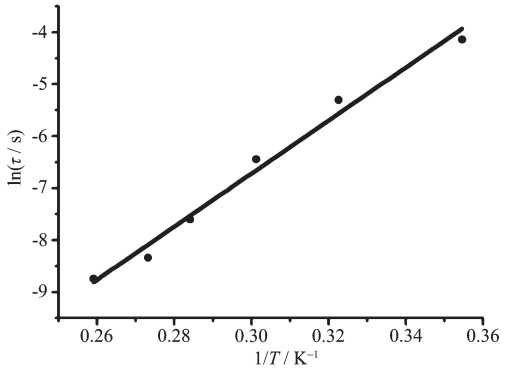

Fig.8　Plot of $\ln\tau$ vs $1/T$ for **2** under 2 000 Oe applied dc field

3　Conclusions

In summary, two new complexes $[M_2L_3(H_2O)]$ (M= Tb (**1**), Dy (**2**)) with Schiff-base ligands were synthesized and characterized by single crystal X-ray diffraction analysis. The structure analysis suggests the present of the magnetic interaction between lanthanide ions. The investigation of magnetic studies confirms the antiferromagnetic interactions between Ln ions. The frequency-dependent out-of-phase signals (χ'') demonstrated the SMM nature of **1** and **2**. We hope that the result is helpful for the study of the magnetic properties of multinuclear lanthanide based SMMs.

References:

[1] Sessoli R, Gatteschi D, Caneschi A, et al. *Nature*, **1993**,**365**(6442):141-143

[2] Sessoli R, Tsai H L, Schake A R, et al. *J. Am. Chem. Soc.*, **1993**,**115**(5):1804-1816

[3] (a)Eppley H J, Tsai H L, de Vries N, et al. *J. Am. Chem. Soc.*, **1995**,**117**(1):301-317
(b)Rinehart J D, Fang M, Evans W J, et al. *Nat. Chem.*, **2011**, **3**(7):538-542
(c)Mannini M, Pineider F, Sainctavit P, et al. *Nat. Mater.*, **2009**,**8**(3):194-197
(d)Hosseini M, Rebi S, Sparkes B M, et al. *Light Sci. Appl.*, **2012**,**1**(12):e40

[4] (a)Bogani L, Wernsdorfer W. *Nat. Mater.*, **2008**,**7**(3):179-186
(b)Mannini M, Pineider F, Danieli C, et al. *Nature*, **2010**,**468** (7332):417-421

[5] (a)Leuenberger M N, Loss D. *Nature*, **2001**,**410**(6830):789-793
(b)Hill S, Edwards R S. *Science*, **2003**,**302**(5647):1015-1018
(c)Timco G A, Carretta S, Troiani F, et al. *Nat. Nanotechnol.*, **2009**,**4**(3):173-178
(d)Thomas L, Lionti F L, Ballou R. *Nature*, **1996**,**383**(6596): 145-147
(e)Wernsdorfer W, Sessoli R. *Science*, **1999**,**284**(5411):133-135

[6] (a)Luzon J, Bernot K, Hewitt I J, et al. *Phys. Rev. Lett.*, **2008**, **100**:247205
(b)Zaleski C M, Depperman E C, Kampf J W, et al. *Angew. Chem. Int. Ed.*, **2004**,**43**:3912-3914
(c)Aronica C, Pilet G, Chastanet G, et al. *Angew. Chem. Int. Ed.*, **2006**,**45**:4659-4662
(d)Christou G, Gatteschi D, Hendrickson D N, et al. *MRS Bull.*, **2000**,**25**:66-71
(e)Gamer M, Lan Y, Roesky P W, et al. *Inorg. Chem.*, **2008**, **47**(15):6581-6583

[7] (a)Joarder B, Mukherjee S, Xue S F, et al. *Inorg. Chem.*, **2014**, **53**(14):7554-7660
(b)Zhang P, Guo Y N, Tang J K. *Coord. Chem. Rev.*, **2013**, **257**(11):1728-1763

[8] (a)Saalfrank R W, Scheurer A, Prakash R. *Inorg. Chem.*, **2007**,**46**(5):1586-1592
(b)Koizumi S, Nihei M, Nakano M. *Inorg. Chem.*, **2005**,**44** (5):1208-1210

[9] (a)Wang H L, Wang B W, Bian Y Z. *Coord. Chem. Rev.*, **2016**, **306**(1):195-216
(b)Abbas G, Lan Y, Kostakis G E. *Inorg. Chem.*, **2010**,**49**(17): 8067-8072
(c)Sessoli R, Powell A K. *Coord. Chem. Rev.*, **2009**,**253**(19): 2328-2341
(d)Papatriantafyllopoulou C, Wernsdorfer W, Abboud K A. *Inorg. Chem.*, **2011**,**50**(2):421-423

[10]Yan P F, Lin P H, Habib F, et al. *Inorg. Chem.*, **2011**,**50** (15):7059-7065

[11](a)Langley S K, Chilton N F, Moubaraki B. *Inorg. Chem. Front.*, **2015**,**2**:867-875
(b)Huo D B, Leng J D, Wang J. *J. Coord. Chem.*, **2017**,**70**: 936-948

[12](a)Dong X Y, Si C D, Fan Y. *Cryst. Growth Des.*, **2016**,**16**: 2062-2073
(b)Wang T, Zhang C, Ju Z. *Dalton Trans.*, **2015**,**44**:6926-6935
(c)Han M L, Bai L, Tang P. *Dalton Trans.*, **2015**,**44**:14673-14685

[13]Alcazar L, Font-Bardia M, Escuer A. *Eur. J. Inorg. Chem.*, **2015**(8):1326-1329

[14](a)Lacelle T, Brunet G, Pialat A. *Dalton Trans.*, **2017**,**46**: 2471-2478
(b)Wang W M, Zhang H X, Wang S Y. *Inorg. Chem.*, **2015**,**54** (24):10610-10622
(c)Wang W M, Guan X F, Liu X D. *Inorg. Chem. Comm.*, **2017**,**79**:8-11
(d)Das L K, Gómez-García C J, Ghosh A. *Dalton Trans.*, **2015**,**44**:1292-1302

[15](a)Floriani C, Solari E, Franceschi F, et al. *Chem. Eur. J.*, **2001**,**7**:3052-3061
(b)Wang C R, Wang S Q, Bo L, et al. *Inorg. Chem. Comm.*, **2017**,**85**:52-55
(c)Liu T Q, Yan P F, Luan F, et al. *Inorg. Chem.*, **2015**,**54** (1):221-228

[16]Wang H L, Liu C X, Liu T, et al. *Dalton Trans.*, **2013**,**42**: 15355-15360

[17]Sheldrick G M. *SHELXL Reference Manual, Version* 5.1, Madison, WI: Bruker Q16 Analytical X-Ray Systems, **1997**.

[18]ZHANG Lu(张璐), ZENG Su-Yuan(曾涑源), LIU Tao(刘涛), et al. *Chinese. J. Inorg. Chem.*(无机化学学报), **2015**,**31**(9): 1761-1773

[19](a)Kan J L, Wang H L, Sun W, et al. *Inorg. Chem.*, **2013**,**52** (15):8505-8510
(b)Zheng Y Z, Lan Y, Wernsdorfer W, et al. *Chem. Eur. J.*, **2009**,**15**:12566-12570
(c)Jiang S D, Wang B W, Su G. *Angew. Chem. Int. Ed.*, **2010**, **122**:7610-7613

[20]Papu B, Pradip B, Amit, K D, et al. *Polyhedron*, **2014**,**75**: 118-126

[21]Lü Z L, Yuan M, Pan F, et al. *Inorg. Chem.*, **2006**,**45**:3538-3548